

# Gravitational Lensing by Black Holes with Multiple Photon Spheres

Guangzhou Guo<sup>a,\*</sup>, Xin Jiang<sup>a,†</sup>, Peng Wang<sup>a,‡</sup> and Houwen Wu<sup>a,b,§</sup>

<sup>a</sup>*Center for Theoretical Physics, College of Physics,  
Sichuan University, Chengdu, 610064, China and*

<sup>b</sup>*Department of Applied Mathematics and Theoretical Physics,  
University of Cambridge, Wilberforce Road, Cambridge, CB3 0WA, UK*

We study gravitational lensing of light by hairy black holes, which, in a certain parameter regime, can possess two photon spheres of different size outside the event horizon. In particular, we focus on higher-order images of a point-like light source and a luminous celestial sphere produced by strong gravitational lensing near photon spheres. Two photon spheres usually triple the number of high-order images of a point-like light source. When a hairy black hole is illuminated by a celestial sphere, two photon spheres would give rise to two critical curves in the black hole image, and the smaller critical curve coincides with the shadow edge. In addition to a set of higher-order images of the celestial sphere outside the shadow edge, two more sets of higher-order images are observed inside and outside the larger critical curve, respectively.

arXiv:2204.13948v2 [gr-qc] 7 May 2022

---

\* [gzguo@stu.scu.edu.cn](mailto:gzguo@stu.scu.edu.cn)

† [xjiang@stu.scu.edu.cn](mailto:xjiang@stu.scu.edu.cn)

‡ [pengw@scu.edu.cn](mailto:pengw@scu.edu.cn)

§ [hw598@damtp.cam.ac.uk](mailto:hw598@damtp.cam.ac.uk)

## CONTENTS

I. Introduction	2
II. Set up	3
III. Numerical Results	6
A. Single-peak potential	7
B. Double-peak potential	8
IV. Conclusions	11
Acknowledgments	13
References	13

## I. INTRODUCTION

One of the elegant predictions of general relativity is the bending of light rays in curved space, which produces an effect similar to that of a lens, and hence is known as gravitational lensing [1–3]. Gravitational lensing has long been an essential tool to address fundamental problems in astrophysics and cosmology. The lensing near relativistic bodies, including a star on an orbit in the Kerr spacetime [4] and an accretion disk around a Schwarzschild black hole [5], were first studied in 1970s. Since then, there have been many works investigating gravitational lensing by the distribution of structures [6–8], dark matter [9–11], dark energy [12–16], quasars [17–20], gravitational waves [21–23] and some other compact objects [24–31]. Recently, the Event Horizon Telescope collaboration achieved an angular resolution sufficient to observe the image of the supermassive black hole in the center of galaxy M87, which ushered us into a new era of studying gravitational lensing in the strong gravity regime [32–39]. In particular, the shadow in black hole images, which is closely related to strong gravitational lensing near photon spheres, has been a subject of great interest to researchers [40–69].

To understand the formation of Hairy Black Holes (HBHs), a novel type of HBH solutions have recently been constructed in Einstein-Maxwell-scalar (EMS) models, where the non-minimal coupling between the scalar field and the electromagnetic field can trigger a tachyonic instability to form spontaneously scalarized HBHs from Reissner-Nordström (RN) black holes [70–74]. Properties of the HBHs have been extensively studied in the literature, e.g., different non-minimal coupling

functions [75–77], massive and self-interacting scalar fields [78, 79], horizonless reflecting stars [80], stability analysis of HBHs [81–85], higher dimensional scalar-tensor models [86], quasinormal modes of HBHs [87, 88], two U(1) fields [89], quasi-topological electromagnetism [90], topology and spacetime structure influences [91], and HBHs in the dS/AdS spacetime [73, 92–94].

Intriguingly, the scalarized HBHs have been found to possess two photon spheres outside the event horizon in certain parameter regions [95, 96]. The existence of two photon spheres can significantly affect the optical appearance of HBHs illuminated by the surrounding accretion disk, e.g., producing bright rings of different radius in the black hole images [95] and noticeably increasing the flux of the observed images [96]. Moreover, the effective potential for a scalar perturbation in the HBHs with two photon spheres was shown to exhibit a double-peak structure, leading to long-lived quasinormal modes [97] and echo signals [98]. It is worth noting that the existence of two photon spheres outside the event horizon has also been reported for dyonic black holes with a quasi-topological electromagnetic term [99] and black holes in massive gravity [100, 101].

Since gravitational lensing plays a key role in observing black holes, we aim to study gravitational lensing by the HBHs with two photon spheres in this paper. The remainder of this paper is organized as follows. After we briefly review the HBH solutions in the Einstein-Maxwell-scalar theory and introduce the observational settings in section II, the lensed images of a point-like light source and a celestial sphere are presented and discussed in section III. Section IV is devoted to our conclusions. We set  $G = c = 1$  throughout the paper.

## II. SET UP

In this section, we briefly review the HBH solutions, discuss the associated geodesic equations and introduce the observational model. Consider an Einstein-Maxwell-scalar theory with an exponential coupling, whose action is given by [70]

$$S = \int d^4x \sqrt{-g} \left[ \mathcal{R} - 2\partial_\mu \phi \partial^\mu \phi - e^{a\phi^2} F_{\mu\nu} F^{\mu\nu} \right], \quad (1)$$

where  $\mathcal{R}$  is the Ricci scalar, the scalar field  $\phi$  is minimally coupled to the metric  $g_{\mu\nu}$  and non-minimally coupled to the electromagnetic field  $A_\mu$ , and  $F_{\mu\nu} = \partial_\mu A_\nu - \partial_\nu A_\mu$  is the electromagnetic field strength tensor. To obtain HBH solutions, it showed that the dimensionless coupling constant  $a$  has to be larger than 1/4 [70]. For the asymptotically flat and spherically symmetric black hole solution ansatz,

$$ds^2 = -N(r)e^{-2\delta(r)} dt^2 + \frac{dr^2}{N(r)} + r^2 (d\theta^2 + \sin^2 \theta d\varphi^2), \quad \mathbf{A} = A_t dt = V(r) dt, \quad (2)$$

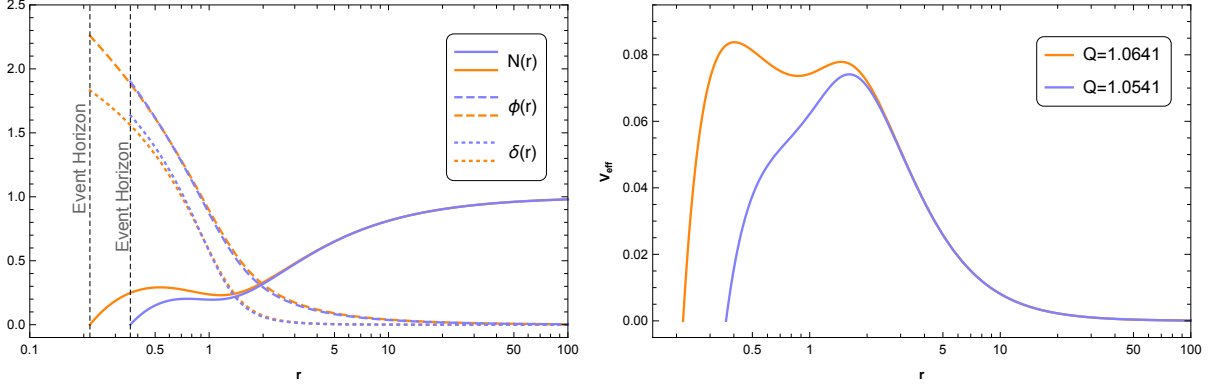


FIG. 1. HBH solutions with  $a = 0.9$  and  $M = 1$  for  $Q = 1.0541$  (blue lines) and  $Q = 1.0641$  (orange lines), and the associated effective potentials as a function of  $r$ . **Left:** The metric functions are plotted outside the event horizon (vertical dashed lines), and the solid, dashed and dotted lines represent  $N(r)$ ,  $\phi(r)$  and  $\delta(r)$ , respectively. **Right:** For the smaller charge (blue line), the effective potential has only a single extremum. For the larger charge (orange line), the effective potential presents a double-peak structure with two local maxima, corresponding to two photon spheres outside the event horizon.

the equations of motion are

$$\begin{aligned}
 2m'(r) - r^2 N(r) \phi'(r)^2 - e^{2\delta(r) + a\phi(r)^2} r^2 V'(r)^2 &= 0, \\
 \delta'(r) + r\phi'(r)^2 &= 0, \\
 \left[ e^{-\delta(r)} r^2 N(r) \phi'(r) \right]' - \alpha e^{\delta(r) + a\phi(r)^2} \phi(r) r^2 V'(r)^2 &= 0, \\
 \left[ e^{\delta(r) + a\phi(r)^2} r^2 V'(r) \right]' &= 0,
 \end{aligned} \tag{3}$$

where the Misner-Sharp mass function  $m(r)$  is defined by  $N(r) \equiv 1 - 2m(r)/r$ , and primes denote derivatives with respect to  $r$ . The last equation in eqn. (3) leads to  $V'(r) = -e^{-\delta(r) - a\phi(r)^2} Q/r^2$ , where the constant  $Q$  can be interpreted as the electric charge of the HBH. Moreover, one can implement boundary conditions at the event horizon of radius  $r_h$  and spatial infinity as

$$\begin{aligned}
 m(r_h) &= \frac{r_h}{2}, \quad \delta(r_h) = \delta_0, \quad \phi(r_h) = \phi_0, \quad V(r_h) = 0, \\
 m(\infty) &= M, \quad \delta(\infty) = 0, \quad \phi(\infty) = 0, \quad V(\infty) = \Psi,
 \end{aligned} \tag{4}$$

where  $\delta_0$  and  $\phi_0$  are two constants characterizing the black hole solution,  $M$  is the Arnowitt-Deser-Misner mass, and  $\Psi$  is the electrostatic potential. In addition, we focus on the fundamental state of the HBH solution, where the scalar field  $\phi(r)$  stays positive outside the event horizon. Note that  $\phi_0 = \delta_0 = 0$  correspond to RN black holes with  $\phi = 0$ . Nevertheless, HBH solutions with a non-trivial scalar field  $\phi$  can exist for non-zero values of  $\phi_0$  and  $\delta_0$ . In this paper, a shooting

method built in the NDSolve function of Wolfram®Mathematica is employed to numerically solve eqn. (3) with the given boundary conditions (4). The metric functions of two HBH solutions with  $a = 0.9$  and  $M = 1$  are presented in FIG. 1, where the blue and orange lines denote  $Q = 1.0541$  and  $Q = 1.0641$ , respectively.

Light rays propagating in the HBH spacetime are described by the geodesic equations

$$\frac{d^2 x^\mu}{d\lambda^2} + \Gamma_{\rho\sigma}^\mu \frac{dx^\rho}{d\lambda} \frac{dx^\sigma}{d\lambda} = 0, \quad (5)$$

where  $\lambda$  is the affine parameter, and  $\Gamma_{\rho\sigma}^\mu$  is the Christoffel symbol. Using  $ds^2 = 0$ , one can rewrite the radial component of the geodesic equations as

$$e^{-2\delta(r)} \left( \frac{dr}{d\lambda} \right)^2 = \frac{1}{b^2} - \frac{e^{-2\delta(r)} N(r)}{r^2}, \quad (6)$$

where we rescale the affine parameter  $\lambda$  as  $\lambda \rightarrow \lambda/|L|$ ,  $b = |L|/E$  is the impact parameter, and  $L$  and  $E$  are the conserved angular momentum and energy of photons, respectively. From eqn. (6), the effective potential governing light rays is defined as

$$V_{\text{eff}}(r) = \frac{e^{-2\delta(r)} N(r)}{r^2}. \quad (7)$$

Unstable circular null geodesics at radius  $r_{\text{ph}}$ , which constitute a photon sphere of radius  $r_{\text{ph}}$ , are determined by

$$V_{\text{eff}}(r_{\text{ph}}) = \frac{1}{b_{\text{ph}}^2}, \quad V'_{\text{eff}}(r) = 0, \quad V''_{\text{eff}}(r_{\text{ph}}) < 0, \quad (8)$$

where  $b_{\text{ph}}$  is the corresponding impact parameter. The effective potential  $V_{\text{eff}}(r)$  of the aforementioned HBH solutions is plotted in the right panel of FIG. 1. Remarkably, it shows that, when the black hole charge is large enough,  $V_{\text{eff}}(r)$  can have two local maxima, leading to a double-peak structure. Consequently, hairy black holes with the double-peak effective potential possess two photon spheres outside the event horizon.

In this paper, we study images of the HBHs illuminated by light sources on a celestial sphere and use the numerical backward ray-tracing method to calculate light rays from an observer to the celestial sphere (or the event horizon). To supply initial conditions for eqn. (6), one considers the 4-momentum of a photon measured by a static observer located at  $(t_o, r_o, \theta_o, 0)$ ,

$$p^{(t)} = -\frac{p_t}{\sqrt{N(r_o)}e^{-\delta(r_o)}}, \quad p^{(r)} = p_r \sqrt{N(r_o)}, \quad p^{(\theta)} = \frac{p_\theta}{r_o}, \quad p^{(\varphi)} = \frac{p_\varphi}{r_o |\sin \theta_o|}, \quad (9)$$

where  $p^\mu = dx^\mu/d\lambda|_{(t_o, r_o, \theta_o, 0)}$ . As in [102], the observation angles  $\alpha$  and  $\beta$  are introduced as

$$\sin \alpha = \frac{p^{(\theta)}}{p^{(t)}}, \quad \tan \beta = \frac{p^{(\varphi)}}{p^{(r)}}, \quad (10)$$

which are determined by the momentum of the photon received by the observer. The Cartesian coordinates  $(x, y)$  of the image plane of the observer is defined by

$$x \equiv -r_o\beta, \quad y \equiv r_o\alpha, \quad (11)$$

where the sign convention for  $\beta$  leads to the minus sign in the  $x$  definition. Note that the zero observation angles  $(0, 0)$  correspond to the direction pointing to the center of the black hole.

The HBH image viewed by the observer is determined by gravitational lensing, which maps the observation angles  $\alpha$  and  $\beta$  to a point in the celestial sphere or the event horizon. Light rays coming from the event horizon correspond to gray pixels in the HBH image, which compose the black hole shadow. On the other hand, the pattern information of the light source is retrieved by light rays connecting the celestial sphere with the observer. Specially, light rays asymptotically originating from photon spheres form critical curves in the HBH image, and hence photons captured near the critical curves will have circled the HBH many times before reaching the observer. As anticipated, higher-order images of the celestial sphere would stack up near the critical curves.

Furthermore, to understand the pattern of the HBH image, we consider multiple images of a point-like light source on the celestial sphere. Due to gravitational lensing, light rays from the point-like light source to the observer can go through different paths to create an infinite series of images. Without loss of generality, we suppose that the observer and the point-like light source are on the equatorial plane and at  $(t_o, r_o, \pi/2, 0)$  and  $(t_s, r_s, \pi/2, \varphi_s)$ , respectively. In this case, the change of angular coordinate  $\Delta\varphi$  of the light rays is given by

$$\Delta\varphi = \begin{cases} \min(\varphi_s, 2\pi - \varphi_s) + n\pi, & n = 0, 2, 4 \dots \\ \max(\varphi_s, 2\pi - \varphi_s) + (n-1)\pi, & n = 1, 3, 5 \dots \end{cases}, \quad (12)$$

where the number  $n$  can be used to label the multiple images. In particular,  $n = 0$  corresponds to the primary image,  $n = 1$  to the secondary image, and  $n > 1$  to the higher-order images.

### III. NUMERICAL RESULTS

To illustrate gravitational lensing by HBHs with single-peak and double-peak effective potentials, we place a luminous celestial sphere at  $r_{CS} = 12M$ . The celestial sphere is concentric with the HBHs and encloses observers. Two static observers, henceforth denoted as  $O$  and  $P$ , are located at  $x_O^\mu = (0, 6M, \pi/2, 0)$  and  $x_P^\mu = (0, 6M, \pi/3, 0)$ , respectively, and their viewing angles capture  $2\pi/3$  of the celestial sphere. From the observers' position, we scan their viewing angles by numerically integrating  $3000 \times 3000$  null geodesics until reaching the celestial sphere or hitting the event

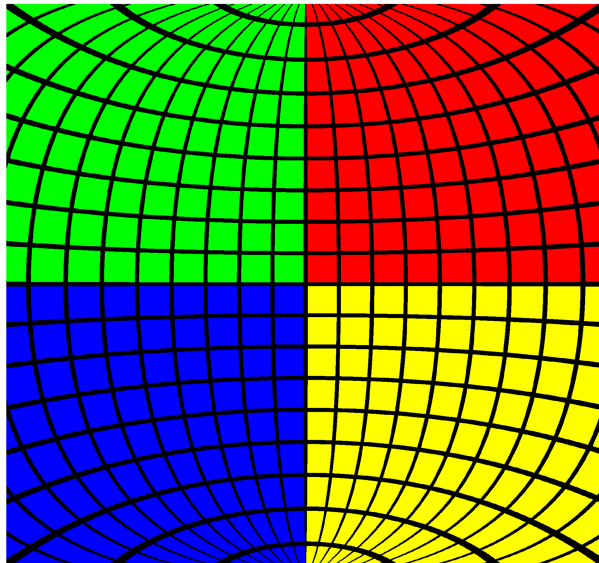


FIG. 2. The observational image of the celestial sphere in the Minkowski spacetime. The observer has a  $2\pi/3$  field of view and is at  $r_O = 6$  on the equatorial plane.

horizon. The light source on the celestial sphere is divided into four quadrants, each of which is painted with a different color. Moreover, we also lay a set of black lines of constant longitude and latitude, with adjacent lines separated by  $\pi/180$ . To illustrate the pattern of the light source, we present the image of the celestial sphere viewed by the observer  $O$  in Minkowski spacetime in FIG. 2. Note that an external view of the celestial sphere can be found in [103, 104]. Without loss of generality, we set  $M = 1$  in this section.

### A. Single-peak potential

We consider gravitational lensing by the HBH with the coupling  $a = 0.9$  and the electric charge  $Q = 1.0541$ , which possesses a single-peak effective potential as shown in the insets of FIG. 3. The single-peak potential indicates a single photon sphere, which plays an important role in the gravitational lensing. In FIG. 3, we plot four light rays connecting a point-like light source on the equator of the celestial sphere with the observer  $O$ , which produce the  $n \leq 3$  images of the light source seen by the observer  $O$ . It displays that strong gravitational lensing near the photon sphere is responsible for the higher-order images of the point-like light source. In addition,  $b^{-2}$  of the light rays are plotted as horizontal lines in the insets of FIG. 3, which shows that the impact parameter of the light rays producing the higher-order images approaches that of the photon sphere

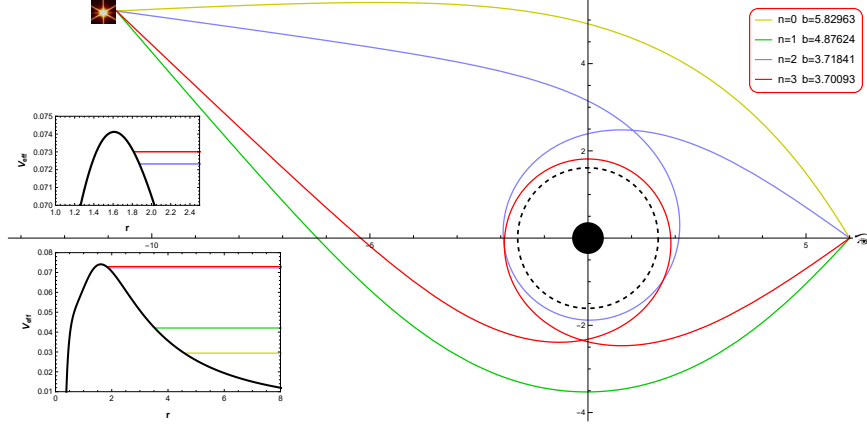


FIG. 3. Light rays producing the primary ( $n = 0$ , yellow line), secondary ( $n = 1$ , green line) and higher-order ( $n = 2$  and  $3$ , blue and red lines) images of a point-like light source on the equatorial plane of the HBH with  $a = 0.9$  and  $Q = 1.0541$ , which has a single-peak potential. The black disk and dashed circle represent the HBH and the photon sphere, respectively. The horizontal lines in the insets denote  $b^{-2}$  of the corresponding light rays, where  $b$  is the impact parameter. The impact parameter of the higher-order images is very close to that of the photon sphere located at the potential peak.

from above in the strong deflection limit with  $n \rightarrow \infty$ . Hence, the higher-order images of the light source lie outside and asymptotically approach the critical curve associated with the photon sphere at the potential peak.

When the HBH is illuminated by the celestial sphere, the black hole images viewed by the observers  $O$  and  $P$  are presented in the upper and lower rows, respectively, in FIG. 4. The gray area in the HBH images is the black hole shadow, whose edge is the critical curve (or “apparent boundary” called by Bardeen [105]). As in the case of point-like light sources, just outside the critical curve lies a sequence of higher-order celestial sphere images, which forms the “photon ring” [106]. To show detailed structure of the photon ring, we magnify the regions bounded by white boxes of the left column in the right column, which display that the higher-order celestial sphere images are self-similar and asymptotically approach the shadow edge.

## B. Double-peak potential

We now investigate gravitational lensing by the HBH with the coupling  $a = 0.85$  and the electric charge  $Q = 1.0603$ , which possesses a double-peak effective potential as shown in the insets of FIG. 5. The two peaks of the potential correspond to two photon spheres of different size outside the event horizon. Note that the inner potential peak is higher than the outer one, which makes effects



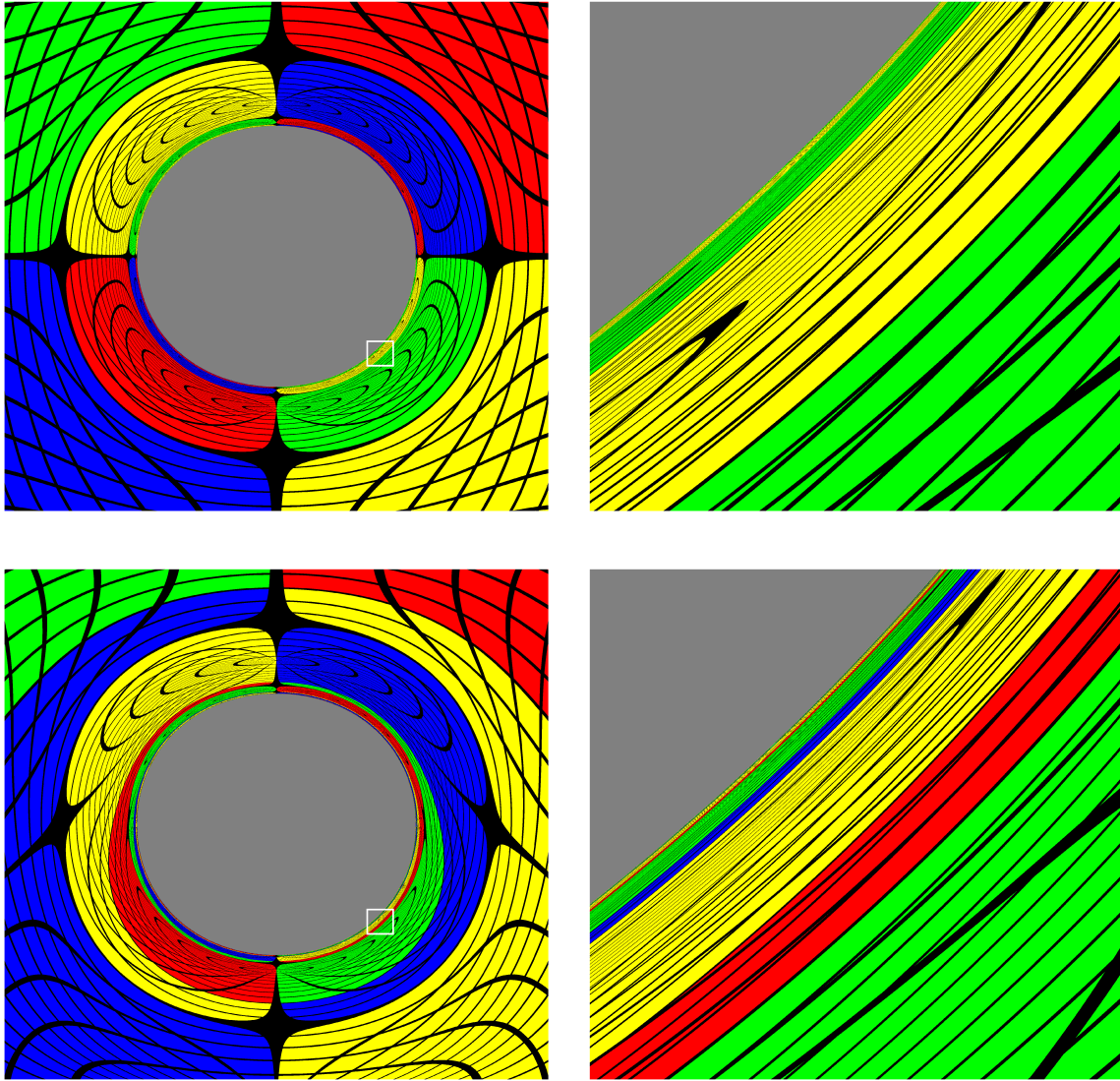


FIG. 4. Images of the HBH, which is illuminated by the celestial sphere, viewed by the observers  $O$  (top row) and  $P$  (bottom row). Here, we take  $a = 0.9$  and  $Q = 1.0541$ , corresponding to a single-peak effective potential. The panels in the right column highlight the regions near the shadow edge (critical curve), which are bounded by white boxes in the left column. There appears a series of higher-order images of the celestial sphere, which asymptotically approaches the shadow edge.

of the smaller photon sphere visible to a distant observer. Owing to the existence of two photon spheres, higher-order images of some light source gravitationally lensed by the HBH can have richer structure than in the single-peak case.

FIG. 5 exhibits light rays travelling from a point-like light source on the equator of the celestial sphere to the observer  $O$ , which produce  $n = 4$  and  $n = 6$  higher-order images of the light source,

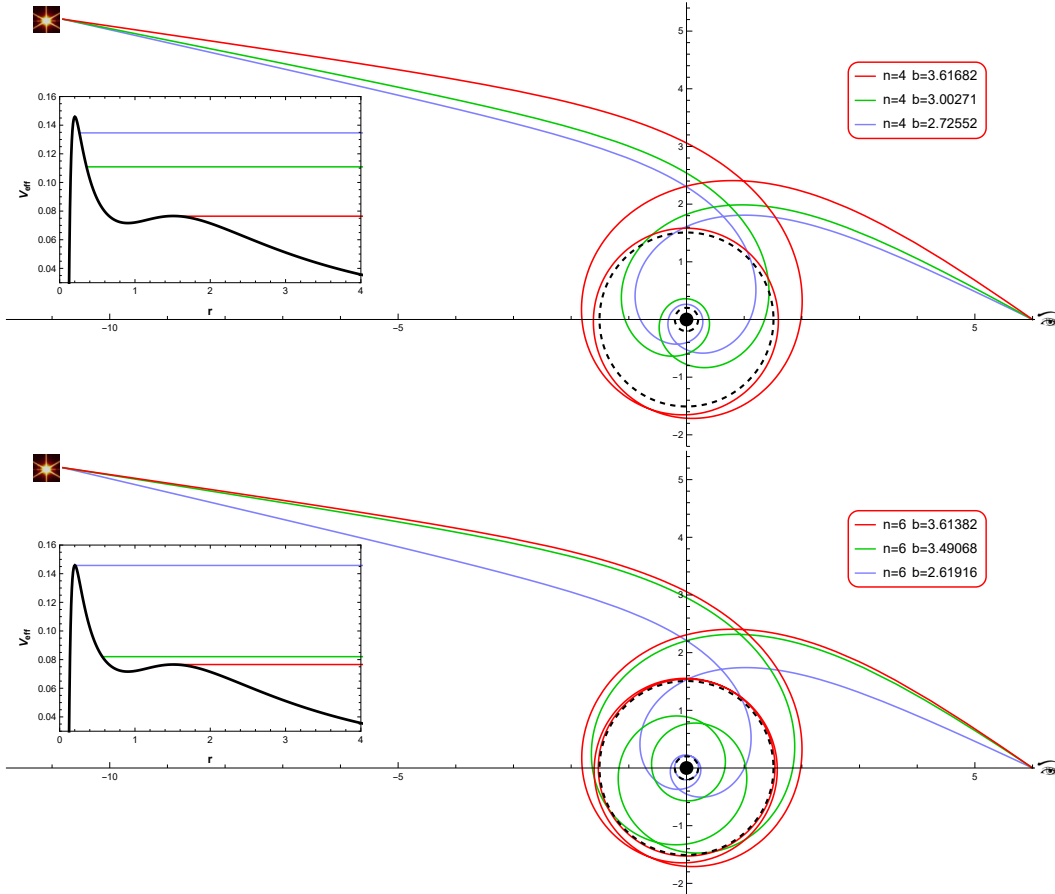


FIG. 5. Light rays producing the  $n = 4$  (top panel) and  $n = 6$  (lower panel) higher-order images of a point-like light source on the equatorial plane of the HBH with  $a = 0.85$  and  $Q = 1.0603$ , which has a double-peak potential. The two dashed circles denote the photon spheres at the potential peaks. In the insets,  $b^{-2}$  of the light rays are plotted as horizontal lines. For each  $n$ , strong gravitational lensing near the photon spheres results in three higher-order images seen by the observer  $O$ .

in the upper and lower panels, respectively. What stands out in this figure is that, for a given  $n$ , three higher-order images can be seen by the observer. On the other hand, a point-like light source only produces one higher-order image with a fixed  $n$  in a HBH of single-peak potential. To gain an insight into the higher-order images, we present  $b^{-2}$  of the light rays as horizontal lines in the insets of FIG. 5. The impact parameter  $b$  of the light rays with the largest/smallest  $b$ , which are displayed as red/blue lines, is slightly larger than  $b$  of the larger/smaller photon sphere, indicating that the light rays of largest/smallest  $b$  may circle around the larger/smaller photon sphere several times before captured by the observer, and produce higher-order images outside the critical curve associated with the larger/smaller photon sphere. When  $n$  is large, the light rays with the largest and smallest  $b$  are expected to be temporarily trapped around the larger and

smaller photon spheres, respectively. More interestingly, the light rays of intermediate  $b$ , which are represented by green lines, can circle around the HBH between the larger and smaller photon spheres. As shown in the insets of FIG. 5, the impact parameter  $b$  of the light rays with the intermediate  $b$  is smaller than that of the larger photon sphere and approaches it with increasing  $n$ . This observation suggests that, these light rays generate higher-order images inside the critical curve associated with the larger photon sphere, and would circle many times around the larger photon sphere in the strong deflection limit when they travel toward or away from the HBH. Note that light rays with  $b$  asymptotically smaller than that of a photon sphere have been analytically discussed in the framework of ultracompact objects [107] and wormholes [108].

If the light source is the celestial sphere, strong gravitational lensing near two photon spheres can leave distinctive imprints on the HBH images. Specifically, light rays asymptotically approaching the two photon spheres yield two critical curves in the HBH images. As explained earlier, higher-order images of the celestial sphere are stacked up near the critical curves. Moreover, the results from the previous paragraph signal that three sets of higher-order images can be observed in the HBH images. In fact, images of the HBH illuminated by the celestial sphere are displayed for the observers  $O$  and  $P$  in the upper and lower rows of FIG. 6, respectively. Similar to the single-peak case, the shadow edge is one critical curve determined by the smaller photon sphere, and one set of higher-order images of the celestial sphere lies just outside the shadow edge. The zoom-in images of the regions bounded by white boxes in the left column are exhibited in the right column, where dashed white lines represent the other critical curve determined by the larger photon sphere. Remarkably, two more sets of higher-order images are spotted inside and outside this critical curve, respectively. In the strong deflection limit, these higher-order images asymptotically approach the critical curve. In contrast to the single-peak case, the photon ring of the images of HBHs with a double-peak potential includes three sets of higher-order images.

#### IV. CONCLUSIONS

In this paper, we investigated lensed images of a point-like light source and a luminous celestial sphere for a class of HBHs in an Einstein-Maxwell-scalar theory, where the scalar field is minimally coupled to the electromagnetic sector. Depending on the HBH parameters, the HBHs can have one or two photon spheres outside the event horizon. For the HBHs with a single photon sphere, strong gravitational lensing around the photon sphere brings about higher-order images of the point-like light source and a set of higher-order images of the celestial sphere just outside the shadow edge.

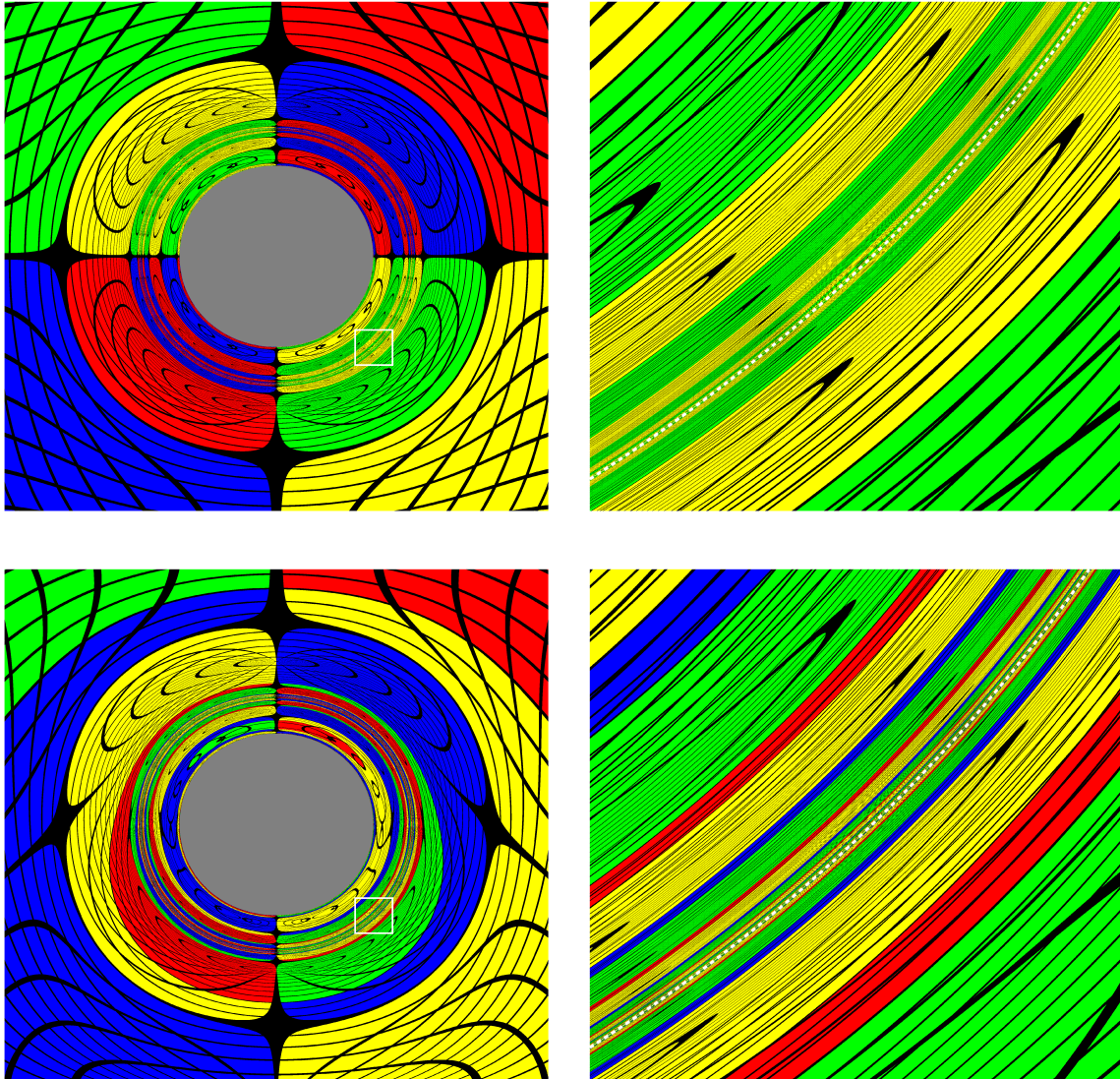


FIG. 6. Images of the celestial sphere gravitationally lensed by the HBH with  $a = 0.85$  and  $Q = 1.0603$ , which has a double-peak potential. The observers  $O$  and  $P$  are considered in the upper and lower rows, respectively. The panels in the right column zoom in the regions bounded by white boxes in the left column. The shadow edge and the dashed white line are the critical curves, which are determined by the smaller and larger photon spheres, respectively. Besides a set of higher-order images just outside the shadow edge, two sets of higher-order images can be seen near the other critical curve.

On the other hand, the existence of an extra photon sphere could triple the number of the higher-order images of the point-like light source. Moreover, three sets of higher-order images of the celestial sphere near two critical curves are observed for the HBHs with two photon spheres. These peculiar signatures provide a powerful tool to search for black holes with multiple photon spheres.

While the shadow size of a black hole may depend on the surrounding astrophysical environment [106, 109], the photon rings, which are composed of higher-order images of the astrophysical source, have been found to be insensitive to the assumed astrophysical source model [110]. Consequently, detections of the photon rings would probe the underlying spacetime in a model-independent way, providing powerful new tests of general relativity and Kerr hypothesis [111–114]. To explore the effects of multiple photon spheres on future detections of the photon rings, it will be of great interest if our analysis can be generalized to more astrophysically realistic models.

### ACKNOWLEDGMENTS

We are grateful to Yiqian Chen for useful discussions and valuable comments. This work is supported in part by NSFC (Grant No. 12105191, 11947225 and 11875196). Houwen Wu is supported by the International Visiting Program for Excellent Young Scholars of Sichuan University.

- 
- [1] F. W. Dyson, A. S. Eddington, and C. Davidson. A Determination of the Deflection of Light by the Sun’s Gravitational Field, from Observations Made at the Total Eclipse of May 29, 1919. *Phil. Trans. Roy. Soc. Lond. A*, 220:291–333, 1920. [doi:10.1098/rsta.1920.0009](https://doi.org/10.1098/rsta.1920.0009). I
  - [2] Albert Einstein. Lens-Like Action of a Star by the Deviation of Light in the Gravitational Field. *Science*, 84:506–507, 1936. [doi:10.1126/science.84.2188.506](https://doi.org/10.1126/science.84.2188.506).
  - [3] A. Eddington. *SPACE, TIME AND GRAVITATION. AN OUTLINE OF THE GENERAL RELATIVITY THEORY*. 1987. I
  - [4] C. T. Cunningham and James M. Bardeen. Optical appearance of a star orbiting an extreme Kerr black hole. *Astrophysical Journal*, 173(3):3032934, 1972. [doi:10.1088/1361-6382/aa9dfc](https://doi.org/10.1088/1361-6382/aa9dfc). I
  - [5] J. P. Luminet. Image of a spherical black hole with thin accretion disk. *Astron. Astrophys.*, 75:228–235, 1979. I
  - [6] Yannick Mellier. Probing the universe with weak lensing. *Ann. Rev. Astron. Astrophys.*, 37:127–189, 1999. [arXiv:astro-ph/9812172](https://arxiv.org/abs/astro-ph/9812172), [doi:10.1146/annurev.astro.37.1.127](https://doi.org/10.1146/annurev.astro.37.1.127). I
  - [7] Matthias Bartelmann and Peter Schneider. Weak gravitational lensing. *Phys. Rept.*, 340:291–472, 2001. [arXiv:astro-ph/9912508](https://arxiv.org/abs/astro-ph/9912508), [doi:10.1016/S0370-1573\(00\)00082-X](https://doi.org/10.1016/S0370-1573(00)00082-X).
  - [8] Catherine Heymans et al. CFHTLenS tomographic weak lensing cosmological parameter constraints: Mitigating the impact of intrinsic galaxy alignments. *Mon. Not. Roy. Astron. Soc.*, 432:2433, 2013. [arXiv:1303.1808](https://arxiv.org/abs/1303.1808), [doi:10.1093/mnras/stt601](https://doi.org/10.1093/mnras/stt601). I
  - [9] Nick Kaiser and Gordon Squires. Mapping the dark matter with weak gravitational lensing. *Astrophys. J.*, 404:441–450, 1993. [doi:10.1086/172297](https://doi.org/10.1086/172297). I

- [10] Douglas Clowe, Marusa Bradac, Anthony H. Gonzalez, Maxim Markevitch, Scott W. Randall, Christine Jones, and Dennis Zaritsky. A direct empirical proof of the existence of dark matter. *Astrophys. J. Lett.*, 648:L109–L113, 2006. [arXiv:astro-ph/0608407](#), [doi:10.1086/508162](#).
- [11] Farruh Atamurotov, Ahmadjon Abdujabbarov, and Wen-Biao Han. Effect of plasma on gravitational lensing by a Schwarzschild black hole immersed in perfect fluid dark matter. *Phys. Rev. D*, 104(8):084015, 2021. [doi:10.1103/PhysRevD.104.084015](#). I
- [12] Marek Biesiada. Strong lensing systems as a probe of dark energy in the universe. *Phys. Rev. D*, 73:023006, 2006. [doi:10.1103/PhysRevD.73.023006](#). I
- [13] Shuo Cao, Marek Biesiada, Rapha Gavazzi, Aleksandra Piórkowska, and Zong-Hong Zhu. Cosmology With Strong-lensing Systems. *Astrophys. J.*, 806:185, 2015. [arXiv:1509.07649](#), [doi:10.1088/0004-637X/806/2/185](#).
- [14] T. M. C. Abbott et al. Dark Energy Survey Year 1 Results: Cosmological constraints from cluster abundances and weak lensing. *Phys. Rev. D*, 102(2):023509, 2020. [arXiv:2002.11124](#), [doi:10.1103/PhysRevD.102.023509](#).
- [15] T. M. C. Abbott et al. Dark Energy Survey Year 3 results: Cosmological constraints from galaxy clustering and weak lensing. *Phys. Rev. D*, 105(2):023520, 2022. [arXiv:2105.13549](#), [doi:10.1103/PhysRevD.105.023520](#).
- [16] Zhen Zhang. Geometrization of light bending and its application to  $SdS_w$  spacetime. *Class. Quant. Grav.*, 39(1):015003, 2022. [arXiv:2112.04149](#), [doi:10.1088/1361-6382/ac38d1](#). I
- [17] Xiaohui Fan et al. The Discovery of a luminous  $z = 5.80$  quasar from the Sloan Digital Sky Survey. *Astron. J.*, 120:1167–1174, 2000. [arXiv:astro-ph/0005414](#), [doi:10.1086/301534](#). I
- [18] Chien Y. Peng, Chris D. Impey, Hans-Walter Rix, Christopher S. Kochanek, Charles R. Keeton, Emilio E. Falco, Joseph Lehar, and Brian A. McLeod. Probing the coevolution of supermassive black holes and galaxies using gravitationally lensed quasar hosts. *Astrophys. J.*, 649:616–634, 2006. [arXiv:astro-ph/0603248](#), [doi:10.1086/506266](#).
- [19] Masamune Oguri and Philip J. Marshall. Gravitationally lensed quasars and supernovae in future wide-field optical imaging surveys. *Mon. Not. Roy. Astron. Soc.*, 405:2579–2593, 2010. [arXiv:1001.2037](#), [doi:10.1111/j.1365-2966.2010.16639.x](#).
- [20] Minghao Yue, Xiaohui Fan, Jinyi Yang, and Feige Wang. Revisiting the Lensed Fraction of High-redshift Quasars. *Astrophys. J.*, 925(2):169, 2022. [arXiv:2112.02821](#), [doi:10.3847/1538-4357/ac409b](#). I
- [21] Uros Seljak and Christopher M. Hirata. Gravitational lensing as a contaminant of the gravity wave signal in CMB. *Phys. Rev. D*, 69:043005, 2004. [arXiv:astro-ph/0310163](#), [doi:10.1103/PhysRevD.69.043005](#). I
- [22] Jose M. Diego, Tom Broadhurst, and George Smoot. Evidence for lensing of gravitational waves from LIGO-Virgo data. *Phys. Rev. D*, 104(10):103529, 2021. [arXiv:2106.06545](#), [doi:10.1103/PhysRevD.104.103529](#).

- [23] Andreas Finke, Stefano Foffa, Francesco Iacovelli, Michele Maggiore, and Michele Mancarella. Probing modified gravitational wave propagation with strongly lensed coalescing binaries. *Phys. Rev. D*, 104(8):084057, 2021. [arXiv:2107.05046](#), [doi:10.1103/PhysRevD.104.084057](#). I
- [24] Fabian Schmidt. Weak Lensing Probes of Modified Gravity. *Phys. Rev. D*, 78:043002, 2008. [arXiv:0805.4812](#), [doi:10.1103/PhysRevD.78.043002](#). I
- [25] Jacek Guzik, Bhuvnesh Jain, and Masahiro Takada. Tests of Gravity from Imaging and Spectroscopic Surveys. *Phys. Rev. D*, 81:023503, 2010. [arXiv:0906.2221](#), [doi:10.1103/PhysRevD.81.023503](#).
- [26] Kai Liao, Zhengxiang Li, Shuo Cao, Marek Biesiada, Xiaogang Zheng, and Zong-Hong Zhu. The Distance Duality Relation From Strong Gravitational Lensing. *Astrophys. J.*, 822(2):74, 2016. [arXiv:1511.01318](#), [doi:10.3847/0004-637X/822/2/74](#).
- [27] Prieslei Goulart. Phantom wormholes in Einstein–Maxwell-dilaton theory. *Class. Quant. Grav.*, 35(2):025012, 2018. [arXiv:1708.00935](#), [doi:10.1088/1361-6382/aa9dfc](#).
- [28] J. R. Nascimento, A. Yu. Petrov, P. J. Porfirio, and A. R. Soares. Gravitational lensing in black-bounce spacetimes. *Phys. Rev. D*, 102(4):044021, 2020. [arXiv:2005.13096](#), [doi:10.1103/PhysRevD.102.044021](#).
- [29] Haroldo C. D. Lima Junior, Jian-Zhi Yang, Luís C. B. Crispino, Pedro V. P. Cunha, and Carlos A. R. Herdeiro. Einstein-Maxwell-dilaton neutral black holes in strong magnetic fields: Topological charge, shadows, and lensing. *Phys. Rev. D*, 105(6):064070, 2022. [arXiv:2112.10802](#), [doi:10.1103/PhysRevD.105.064070](#).
- [30] Shafqat Ul Islam, Jitendra Kumar, and Sushant G. Ghosh. Strong gravitational lensing by rotating Simpson-Visser black holes. *JCAP*, 10:013, 2021. [arXiv:2104.00696](#), [doi:10.1088/1475-7516/2021/10/013](#).
- [31] Naoki Tsukamoto. Retrolensing by two photon spheres of a black-bounce spacetime. *Phys. Rev. D*, 105(8):084036, 2022. [arXiv:2202.09641](#), [doi:10.1103/PhysRevD.105.084036](#). I
- [32] Kazunori Akiyama et al. First M87 Event Horizon Telescope Results. I. The Shadow of the Supermassive Black Hole. *Astrophys. J. Lett.*, 875:L1, 2019. [arXiv:1906.11238](#), [doi:10.3847/2041-8213/ab0ec7](#). I
- [33] Kazunori Akiyama et al. First M87 Event Horizon Telescope Results. II. Array and Instrumentation. *Astrophys. J. Lett.*, 875(1):L2, 2019. [arXiv:1906.11239](#), [doi:10.3847/2041-8213/ab0c96](#).
- [34] Kazunori Akiyama et al. First M87 Event Horizon Telescope Results. III. Data Processing and Calibration. *Astrophys. J. Lett.*, 875(1):L3, 2019. [arXiv:1906.11240](#), [doi:10.3847/2041-8213/ab0c57](#).
- [35] Kazunori Akiyama et al. First M87 Event Horizon Telescope Results. IV. Imaging the Central Supermassive Black Hole. *Astrophys. J. Lett.*, 875(1):L4, 2019. [arXiv:1906.11241](#), [doi:10.3847/2041-8213/ab0e85](#).
- [36] Kazunori Akiyama et al. First M87 Event Horizon Telescope Results. V. Physical Origin of the Asymmetric Ring. *Astrophys. J. Lett.*, 875(1):L5, 2019. [arXiv:1906.11242](#), [doi:10.3847/2041-8213/](#)

ab0f43.

- [37] Kazunori Akiyama et al. First M87 Event Horizon Telescope Results. VI. The Shadow and Mass of the Central Black Hole. *Astrophys. J. Lett.*, 875(1):L6, 2019. [arXiv:1906.11243](#), [doi:10.3847/2041-8213/ab1141](#).
- [38] Kazunori Akiyama et al. First M87 Event Horizon Telescope Results. VII. Polarization of the Ring. *Astrophys. J. Lett.*, 910(1):L12, 2021. [arXiv:2105.01169](#), [doi:10.3847/2041-8213/abe71d](#).
- [39] Kazunori Akiyama et al. First M87 Event Horizon Telescope Results. VIII. Magnetic Field Structure near The Event Horizon. *Astrophys. J. Lett.*, 910(1):L13, 2021. [arXiv:2105.01173](#), [doi:10.3847/2041-8213/abe4de](#). I
- [40] Heino Falcke, Fulvio Melia, and Eric Agol. Viewing the shadow of the black hole at the galactic center. *Astrophys. J. Lett.*, 528:L13, 2000. [arXiv:astro-ph/9912263](#), [doi:10.1086/312423](#). I
- [41] K. S. Virbhadra and George F. R. Ellis. Schwarzschild black hole lensing. *Phys. Rev. D*, 62:084003, 2000. [arXiv:astro-ph/9904193](#), [doi:10.1103/PhysRevD.62.084003](#).
- [42] Clarissa-Marie Claudel, K. S. Virbhadra, and G. F. R. Ellis. The Geometry of photon surfaces. *J. Math. Phys.*, 42:818–838, 2001. [arXiv:gr-qc/0005050](#), [doi:10.1063/1.1308507](#).
- [43] Ernesto F. Eiroa, Gustavo E. Romero, and Diego F. Torres. Reissner-Nordstrom black hole lensing. *Phys. Rev. D*, 66:024010, 2002. [arXiv:gr-qc/0203049](#), [doi:10.1103/PhysRevD.66.024010](#).
- [44] K. S. Virbhadra. Relativistic images of Schwarzschild black hole lensing. *Phys. Rev. D*, 79:083004, 2009. [arXiv:0810.2109](#), [doi:10.1103/PhysRevD.79.083004](#).
- [45] Akifumi Yumoto, Daisuke Nitta, Takeshi Chiba, and Naoshi Sugiyama. Shadows of Multi-Black Holes: Analytic Exploration. *Phys. Rev. D*, 86:103001, 2012. [arXiv:1208.0635](#), [doi:10.1103/PhysRevD.86.103001](#).
- [46] Shao-Wen Wei and Yu-Xiao Liu. Observing the shadow of Einstein-Maxwell-Dilaton-Axion black hole. *JCAP*, 11:063, 2013. [arXiv:1311.4251](#), [doi:10.1088/1475-7516/2013/11/063](#).
- [47] Alexander F. Zakharov. Constraints on a charge in the Reissner-Nordström metric for the black hole at the Galactic Center. *Phys. Rev. D*, 90(6):062007, 2014. [arXiv:1407.7457](#), [doi:10.1103/PhysRevD.90.062007](#).
- [48] Farruh Atamurotov, Sushant G. Ghosh, and Bobomurat Ahmedov. Horizon structure of rotating Einstein–Born–Infeld black holes and shadow. *Eur. Phys. J. C*, 76(5):273, 2016. [arXiv:1506.03690](#), [doi:10.1140/epjc/s10052-016-4122-9](#).
- [49] Pedro V. P. Cunha, Carlos A. R. Herdeiro, Burkhard Kleihaus, Jutta Kunz, and Eugen Radu. Shadows of Einstein–dilaton–Gauss–Bonnet black holes. *Phys. Lett. B*, 768:373–379, 2017. [arXiv:1701.00079](#), [doi:10.1016/j.physletb.2017.03.020](#).
- [50] Sara Dastan, Reza Saffari, and Saheb Soroushfar. Shadow of a Kerr-Sen dilaton-axion Black Hole. 10 2016. [arXiv:1610.09477](#).
- [51] Muhammed Amir, Balendra Pratap Singh, and Sushant G. Ghosh. Shadows of rotating five-dimensional charged EMCS black holes. *Eur. Phys. J. C*, 78(5):399, 2018. [arXiv:1707.09521](#),



- [doi:10.1140/epjc/s10052-018-5872-3](https://doi.org/10.1140/epjc/s10052-018-5872-3).
- [52] Mingzhi Wang, Songbai Chen, and Jiliang Jing. Shadow casted by a Konoplya-Zhidenko rotating non-Kerr black hole. *JCAP*, 10:051, 2017. [arXiv:1707.09451](https://arxiv.org/abs/1707.09451), [doi:10.1088/1475-7516/2017/10/051](https://doi.org/10.1088/1475-7516/2017/10/051).
- [53] Ali Övgün, İzzet Sakalli, and Joel Saavedra. Shadow cast and Deflection angle of Kerr-Newman-Kasuya spacetime. *JCAP*, 10:041, 2018. [arXiv:1807.00388](https://arxiv.org/abs/1807.00388), [doi:10.1088/1475-7516/2018/10/041](https://doi.org/10.1088/1475-7516/2018/10/041).
- [54] Volker Perlick, Oleg Yu. Tsupko, and Gennady S. Bisnovatyi-Kogan. Black hole shadow in an expanding universe with a cosmological constant. *Phys. Rev. D*, 97(10):104062, 2018. [arXiv:1804.04898](https://arxiv.org/abs/1804.04898), [doi:10.1103/PhysRevD.97.104062](https://doi.org/10.1103/PhysRevD.97.104062).
- [55] Rahul Kumar, Sushant G. Ghosh, and Anzhong Wang. Shadow cast and deflection of light by charged rotating regular black holes. *Phys. Rev. D*, 100(12):124024, 2019. [arXiv:1912.05154](https://arxiv.org/abs/1912.05154), [doi:10.1103/PhysRevD.100.124024](https://doi.org/10.1103/PhysRevD.100.124024).
- [56] Tao Zhu, Qiang Wu, Mubasher Jamil, and Kimet Jusufi. Shadows and deflection angle of charged and slowly rotating black holes in Einstein-Æther theory. *Phys. Rev. D*, 100(4):044055, 2019. [arXiv:1906.05673](https://arxiv.org/abs/1906.05673), [doi:10.1103/PhysRevD.100.044055](https://doi.org/10.1103/PhysRevD.100.044055).
- [57] Liang Ma and H. Lu. Bounds on photon spheres and shadows of charged black holes in Einstein-Gauss-Bonnet-Maxwell gravity. *Phys. Lett. B*, 807:135535, 2020. [arXiv:1912.05569](https://arxiv.org/abs/1912.05569), [doi:10.1016/j.physletb.2020.135535](https://doi.org/10.1016/j.physletb.2020.135535).
- [58] Akash K. Mishra, Sumanta Chakraborty, and Sudipta Sarkar. Understanding photon sphere and black hole shadow in dynamically evolving spacetimes. *Phys. Rev. D*, 99(10):104080, 2019. [arXiv:1903.06376](https://arxiv.org/abs/1903.06376), [doi:10.1103/PhysRevD.99.104080](https://doi.org/10.1103/PhysRevD.99.104080).
- [59] Xiao-Xiong Zeng, Hai-Qing Zhang, and Hongbao Zhang. Shadows and photon spheres with spherical accretions in the four-dimensional Gauss-Bonnet black hole. *Eur. Phys. J. C*, 80(9):872, 2020. [arXiv:2004.12074](https://arxiv.org/abs/2004.12074), [doi:10.1140/epjc/s10052-020-08449-y](https://doi.org/10.1140/epjc/s10052-020-08449-y).
- [60] Xiao-Xiong Zeng and Hai-Qing Zhang. Influence of quintessence dark energy on the shadow of black hole. *Eur. Phys. J. C*, 80(11):1058, 2020. [arXiv:2007.06333](https://arxiv.org/abs/2007.06333), [doi:10.1140/epjc/s10052-020-08656-7](https://doi.org/10.1140/epjc/s10052-020-08656-7).
- [61] Xin Qin, Songbai Chen, and Jiliang Jing. Image of a regular phantom black hole and its luminosity under spherical accretions. 11 2020. [arXiv:2011.04310](https://arxiv.org/abs/2011.04310).
- [62] K. Saurabh and Kimet Jusufi. Imprints of dark matter on black hole shadows using spherical accretions. *Eur. Phys. J. C*, 81(6):490, 2021. [arXiv:2009.10599](https://arxiv.org/abs/2009.10599), [doi:10.1140/epjc/s10052-021-09280-9](https://doi.org/10.1140/epjc/s10052-021-09280-9).
- [63] Rittick Roy and Sayan Chakrabarti. Study on black hole shadows in asymptotically de Sitter spacetimes. *Phys. Rev. D*, 102(2):024059, 2020. [arXiv:2003.14107](https://arxiv.org/abs/2003.14107), [doi:10.1103/PhysRevD.102.024059](https://doi.org/10.1103/PhysRevD.102.024059).
- [64] Peng-Cheng Li, Minyong Guo, and Bin Chen. Shadow of a Spinning Black Hole in an Expanding Universe. *Phys. Rev. D*, 101(8):084041, 2020. [arXiv:2001.04231](https://arxiv.org/abs/2001.04231), [doi:10.1103/PhysRevD.101.084041](https://doi.org/10.1103/PhysRevD.101.084041).
- [65] Rahul Kumar, Sushant G. Ghosh, and Anzhong Wang. Gravitational deflection of light and shadow cast by rotating Kalb-Ramond black holes. *Phys. Rev. D*, 101(10):104001, 2020. [arXiv:2001.00460](https://arxiv.org/abs/2001.00460),

- [doi:10.1103/PhysRevD.101.104001](https://doi.org/10.1103/PhysRevD.101.104001).
- [66] Ming Zhang and Jie Jiang. Shadows of accelerating black holes. *Phys. Rev. D*, 103(2):025005, 2021. [arXiv:2010.12194](https://arxiv.org/abs/2010.12194), [doi:10.1103/PhysRevD.103.025005](https://doi.org/10.1103/PhysRevD.103.025005).
- [67] Gonzalo J. Olmo, Diego Rubiera-Garcia, and Diego Sáez-Chillón Gómez. New light rings from multiple critical curves as observational signatures of black hole mimickers. *Phys. Lett. B*, 829:137045, 2022. [arXiv:2110.10002](https://arxiv.org/abs/2110.10002), [doi:10.1016/j.physletb.2022.137045](https://doi.org/10.1016/j.physletb.2022.137045).
- [68] Merce Guerrero, Gonzalo J. Olmo, Diego Rubiera-Garcia, and Diego Gómez Sáez-Chillón. Light ring images of double photon spheres in black hole and wormhole spacetimes. *Phys. Rev. D*, 105(8):084057, 2022. [arXiv:2202.03809](https://arxiv.org/abs/2202.03809), [doi:10.1103/PhysRevD.105.084057](https://doi.org/10.1103/PhysRevD.105.084057).
- [69] K. S. Virbhadra. Distortions of images of Schwarzschild lensing. 4 2022. [arXiv:2204.01879](https://arxiv.org/abs/2204.01879). I
- [70] Carlos A.R. Herdeiro, Eugen Radu, Nicolas Sanchis-Gual, and José A. Font. Spontaneous Scalarization of Charged Black Holes. *Phys. Rev. Lett.*, 121(10):101102, 2018. [arXiv:1806.05190](https://arxiv.org/abs/1806.05190), [doi:10.1103/PhysRevLett.121.101102](https://doi.org/10.1103/PhysRevLett.121.101102). I, II, II
- [71] R. A. Konoplya and A. Zhidenko. Analytical representation for metrics of scalarized Einstein-Maxwell black holes and their shadows. *Phys. Rev. D*, 100(4):044015, 2019. [arXiv:1907.05551](https://arxiv.org/abs/1907.05551), [doi:10.1103/PhysRevD.100.044015](https://doi.org/10.1103/PhysRevD.100.044015).
- [72] Peng Wang, Houwen Wu, and Haitang Yang. Scalarized Einstein-Born-Infeld black holes. *Phys. Rev. D*, 103(10):104012, 2021. [arXiv:2012.01066](https://arxiv.org/abs/2012.01066), [doi:10.1103/PhysRevD.103.104012](https://doi.org/10.1103/PhysRevD.103.104012).
- [73] Guangzhou Guo, Peng Wang, Houwen Wu, and Haitang Yang. Scalarized Einstein–Maxwell-scalar black holes in anti-de Sitter spacetime. *Eur. Phys. J. C*, 81(10):864, 2021. [arXiv:2102.04015](https://arxiv.org/abs/2102.04015), [doi:10.1140/epjc/s10052-021-09614-7](https://doi.org/10.1140/epjc/s10052-021-09614-7). I
- [74] Guangzhou Guo, Peng Wang, Houwen Wu, and Haitang Yang. Thermodynamics and phase structure of an Einstein-Maxwell-scalar model in extended phase space. *Phys. Rev. D*, 105(6):064069, 2022. [arXiv:2107.04467](https://arxiv.org/abs/2107.04467), [doi:10.1103/PhysRevD.105.064069](https://doi.org/10.1103/PhysRevD.105.064069). I
- [75] Pedro G. S. Fernandes, Carlos A. R. Herdeiro, Alexandre M. Pombo, Eugen Radu, and Nicolas Sanchis-Gual. Spontaneous Scalarisation of Charged Black Holes: Coupling Dependence and Dynamical Features. *Class. Quant. Grav.*, 36(13):134002, 2019. [Erratum: *Class.Quant.Grav.* 37, 049501 (2020)]. [arXiv:1902.05079](https://arxiv.org/abs/1902.05079), [doi:10.1088/1361-6382/ab23a1](https://doi.org/10.1088/1361-6382/ab23a1). I
- [76] Pedro G.S. Fernandes, Carlos A.R. Herdeiro, Alexandre M. Pombo, Eugen Radu, and Nicolas Sanchis-Gual. Charged black holes with axionic-type couplings: Classes of solutions and dynamical scalarization. *Phys. Rev. D*, 100(8):084045, 2019. [arXiv:1908.00037](https://arxiv.org/abs/1908.00037), [doi:10.1103/PhysRevD.100.084045](https://doi.org/10.1103/PhysRevD.100.084045).
- [77] Jose Luis Blázquez-Salcedo, Carlos A.R. Herdeiro, Jutta Kunz, Alexandre M. Pombo, and Eugen Radu. Einstein-Maxwell-scalar black holes: the hot, the cold and the bald. *Phys. Lett. B*, 806:135493, 2020. [arXiv:2002.00963](https://arxiv.org/abs/2002.00963), [doi:10.1016/j.physletb.2020.135493](https://doi.org/10.1016/j.physletb.2020.135493). I
- [78] De-Cheng Zou and Yun Soo Myung. Scalarized charged black holes with scalar mass term. *Phys. Rev. D*, 100(12):124055, 2019. [arXiv:1909.11859](https://arxiv.org/abs/1909.11859), [doi:10.1103/PhysRevD.100.124055](https://doi.org/10.1103/PhysRevD.100.124055). I
- [79] Pedro G.S. Fernandes. Einstein-Maxwell-scalar black holes with massive and self-interacting scalar

- hair. *Phys. Dark Univ.*, 30:100716, 2020. [arXiv:2003.01045](#), [doi:10.1016/j.dark.2020.100716](#). I
- [80] Yan Peng. Scalarization of horizonless reflecting stars: neutral scalar fields non-minimally coupled to Maxwell fields. *Phys. Lett. B*, 804:135372, 2020. [arXiv:1912.11989](#), [doi:10.1016/j.physletb.2020.135372](#). I
- [81] Yun Soo Myung and De-Cheng Zou. Instability of Reissner–Nordström black hole in Einstein–Maxwell-scalar theory. *Eur. Phys. J. C*, 79(3):273, 2019. [arXiv:1808.02609](#), [doi:10.1140/epjc/s10052-019-6792-6](#). I
- [82] Yun Soo Myung and De-Cheng Zou. Stability of scalarized charged black holes in the Einstein–Maxwell–Scalar theory. *Eur. Phys. J. C*, 79(8):641, 2019. [arXiv:1904.09864](#), [doi:10.1140/epjc/s10052-019-7176-7](#).
- [83] De-Cheng Zou and Yun Soo Myung. Radial perturbations of the scalarized black holes in Einstein–Maxwell-conformally coupled scalar theory. *Phys. Rev. D*, 102(6):064011, 2020. [arXiv:2005.06677](#), [doi:10.1103/PhysRevD.102.064011](#).
- [84] Yun Soo Myung and De-Cheng Zou. Onset of rotating scalarized black holes in Einstein–Chern–Simons–Scalar theory. *Phys. Lett. B*, 814:136081, 2021. [arXiv:2012.02375](#), [doi:10.1016/j.physletb.2021.136081](#).
- [85] Zhan-Feng Mai and Run-Qiu Yang. Stability analysis of a charged black hole with a nonlinear complex scalar field. *Phys. Rev. D*, 104(4):044008, 2021. [arXiv:2101.00026](#), [doi:10.1103/PhysRevD.104.044008](#). I
- [86] Dumitru Astefanesei, Carlos Herdeiro, João Oliveira, and Eugen Radu. Higher dimensional black hole scalarization. *JHEP*, 09:186, 2020. [arXiv:2007.04153](#), [doi:10.1007/JHEP09\(2020\)186](#). I
- [87] Yun Soo Myung and De-Cheng Zou. Quasinormal modes of scalarized black holes in the Einstein–Maxwell–Scalar theory. *Phys. Lett. B*, 790:400–407, 2019. [arXiv:1812.03604](#), [doi:10.1016/j.physletb.2019.01.046](#). I
- [88] Jose Luis Blázquez-Salcedo, Carlos A.R. Herdeiro, Sarah Kahlen, Jutta Kunz, Alexandre M. Pombo, and Eugen Radu. Quasinormal modes of hot, cold and bald Einstein–Maxwell-scalar black holes. 8 2020. [arXiv:2008.11744](#). I
- [89] Yun Soo Myung and De-Cheng Zou. Scalarized charged black holes in the Einstein–Maxwell–Scalar theory with two  $U(1)$  fields. *Phys. Lett. B*, 811:135905, 2020. [arXiv:2009.05193](#), [doi:10.1016/j.physletb.2020.135905](#). I
- [90] Yun Soo Myung and De-Cheng Zou. Scalarized black holes in the Einstein–Maxwell-scalar theory with a quasitopological term. *Phys. Rev. D*, 103(2):024010, 2021. [arXiv:2011.09665](#), [doi:10.1103/PhysRevD.103.024010](#). I
- [91] Hong Guo, Xiao-Mei Kuang, Eleftherios Papantonopoulos, and Bin Wang. Topology and spacetime structure influences on black hole scalarization. 12 2020. [arXiv:2012.11844](#). I
- [92] Yves Brihaye, Betti Hartmann, Nathália Pio Aprile, and Jon Urrestilla. Scalarization of asymptotically anti-de Sitter black holes with applications to holographic phase transitions. *Phys. Rev. D*,

- 101(12):124016, 2020. [arXiv:1911.01950](#), [doi:10.1103/PhysRevD.101.124016](#). I
- [93] Yves Brihaye, Carlos Herdeiro, and Eugen Radu. Black Hole Spontaneous Scalarisation with a Positive Cosmological Constant. *Phys. Lett. B*, 802:135269, 2020. [arXiv:1910.05286](#), [doi:10.1016/j.physletb.2020.135269](#).
- [94] Cheng-Yong Zhang, Peng Liu, Yunqi Liu, Chao Niu, and Bin Wang. Dynamical charged black hole spontaneous scalarization in Anti-de Sitter spacetimes. 3 2021. [arXiv:2103.13599](#). I
- [95] Qingyu Gan, Peng Wang, Houwen Wu, and Haitang Yang. Photon spheres and spherical accretion image of a hairy black hole. *Phys. Rev. D*, 104(2):024003, 2021. [arXiv:2104.08703](#), [doi:10.1103/PhysRevD.104.024003](#). I
- [96] Qingyu Gan, Peng Wang, Houwen Wu, and Haitang Yang. Photon ring and observational appearance of a hairy black hole. *Phys. Rev. D*, 104(4):044049, 2021. [arXiv:2105.11770](#), [doi:10.1103/PhysRevD.104.044049](#). I
- [97] Guangzhou Guo, Peng Wang, Houwen Wu, and Haitang Yang. Quasinormal Modes of Black Holes with Multiple Photon Spheres. 12 2021. [arXiv:2112.14133](#). I
- [98] Guangzhou Guo, Peng Wang, Houwen Wu, and Haitang Yang. Echoes from Hairy Black Holes. 4 2022. [arXiv:2204.00982](#). I
- [99] Hai-Shan Liu, Zhan-Feng Mai, Yue-Zhou Li, and H. Lü. Quasi-topological Electromagnetism: Dark Energy, Dyonic Black Holes, Stable Photon Spheres and Hidden Electromagnetic Duality. *Sci. China Phys. Mech. Astron.*, 63:240411, 2020. [arXiv:1907.10876](#), [doi:10.1007/s11433-019-1446-1](#). I
- [100] Claudia de Rham, Gregory Gabadadze, and Andrew J. Tolley. Resummation of Massive Gravity. *Phys. Rev. Lett.*, 106:231101, 2011. [arXiv:1011.1232](#), [doi:10.1103/PhysRevLett.106.231101](#). I
- [101] Ruifeng Dong and Dejan Stojkovic. Gravitational wave echoes from black holes in massive gravity. *Phys. Rev. D*, 103(2):024058, 2021. [arXiv:2011.04032](#), [doi:10.1103/PhysRevD.103.024058](#). I
- [102] Pedro V. P. Cunha, Carlos A. R. Herdeiro, Eugen Radu, and Helgi F. Runarsson. Shadows of Kerr black holes with and without scalar hair. *Int. J. Mod. Phys. D*, 25(09):1641021, 2016. [arXiv:1605.08293](#), [doi:10.1142/S0218271816410212](#). II
- [103] Andy Bohn, William Thrope, Fran Hébert, Katherine Henriksson, Darius Bunandar, Mark A. Scheel, and Nicholas W. Taylor. What does a binary black hole merger look like? *Class. Quant. Grav.*, 32(6):065002, 2015. [arXiv:1410.7775](#), [doi:10.1088/0264-9381/32/6/065002](#). III
- [104] Pedro V. P. Cunha, Carlos A. R. Herdeiro, Eugen Radu, and Helgi F. Runarsson. Shadows of Kerr black holes with scalar hair. *Phys. Rev. Lett.*, 115(21):211102, 2015. [arXiv:1509.00021](#), [doi:10.1103/PhysRevLett.115.211102](#). III
- [105] J. M. Bardeen. Timelike and null geodesics in the Kerr metric. In *Les Houches Summer School of Theoretical Physics: Black Holes*, 1973. III A
- [106] Samuel E. Gralla, Daniel E. Holz, and Robert M. Wald. Black Hole Shadows, Photon Rings, and Lensing Rings. *Phys. Rev. D*, 100(2):024018, 2019. [arXiv:1906.00873](#), [doi:10.1103/PhysRevD.100.024018](#). III A, IV

- [107] Rajibul Shaikh, Pritam Banerjee, Suvankar Paul, and Tapobrata Sarkar. Analytical approach to strong gravitational lensing from ultracompact objects. *Phys. Rev. D*, 99(10):104040, 2019. [arXiv:1903.08211](#), [doi:10.1103/PhysRevD.99.104040](#). III B
- [108] Naoki Tsukamoto. Gravitational lensing by two photon spheres in a black-bounce spacetime in strong deflection limits. 5 2021. [arXiv:2105.14336](#). III B
- [109] Andrew Chael, Michael D. Johnson, and Alexandru Lupsasca. Observing the Inner Shadow of a Black Hole: A Direct View of the Event Horizon. *Astrophys. J.*, 918(1):6, 2021. [arXiv:2106.00683](#), [doi:10.3847/1538-4357/ac09ee](#). IV
- [110] Samuel E. Gralla, Alexandru Lupsasca, and Daniel P. Marrone. The shape of the black hole photon ring: A precise test of strong-field general relativity. *Phys. Rev. D*, 102(12):124004, 2020. [arXiv:2008.03879](#), [doi:10.1103/PhysRevD.102.124004](#). IV
- [111] Michael D. Johnson et al. Universal interferometric signatures of a black hole’s photon ring. *Sci. Adv.*, 6(12):eaaz1310, 2020. [arXiv:1907.04329](#), [doi:10.1126/sciadv.aaz1310](#). IV
- [112] Shahar Hadar, Michael D. Johnson, Alexandru Lupsasca, and George N. Wong. Photon Ring Auto-correlations. *Phys. Rev. D*, 103(10):104038, 2021. [arXiv:2010.03683](#), [doi:10.1103/PhysRevD.103.104038](#).
- [113] Maciek Wielgus. Photon rings of spherically symmetric black holes and robust tests of non-Kerr metrics. *Phys. Rev. D*, 104(12):124058, 2021. [arXiv:2109.10840](#), [doi:10.1103/PhysRevD.104.124058](#).
- [114] Avery E. Broderick, Paul Tiede, Dominic W. Pesce, and Roman Gold. Measuring Spin from Relative Photon-ring Sizes. *Astrophys. J.*, 927(1):6, 2022. [arXiv:2105.09962](#), [doi:10.3847/1538-4357/ac4970](#). IV